

# Elastic proton scattering at intermediate energies as a probe of the $^{6,8}\text{He}$ nuclear matter densities

Le Xuan Chung<sup>1</sup>, Oleg A. Kiselev<sup>2</sup>, Dao T. Khoa<sup>1</sup>, and Peter Egelhof<sup>2</sup>

<sup>1</sup>*Institute for Nuclear Science and Technique, VINATOM*

*179 Hoang Quoc Viet Road, Cau Giay, Hanoi, Vietnam.*

<sup>2</sup>*GSI Helmholtzzentrum für Schwerionenforschung, 64291 Darmstadt, Germany.*

(Dated: November 5, 2018)

## Abstract

The Glauber model analysis of the elastic  $^{6,8}\text{He}+p$  scattering data at energies around 700 MeV/nucleon, measured in two separate experiments at GSI-Darmstadt, has been done using several phenomenological parametrizations of the nuclear matter density. By taking into account the new data points measured at the high momentum transfer, the nuclear matter radii of  $^{6,8}\text{He}$  were accurately determined from the Glauber model analysis of the data, with the spin-orbital interaction explicitly taken into account. The well-known geometry for the core and dineutron halo has been used with the new parametrizations of the  $^6\text{He}$  density to extract the detailed information on the structure of  $^6\text{He}$  in terms of the core and dineutron halo radii. An enhanced sensitivity of the data measured at the high momentum transfer to the core part of the  $^{6,8}\text{He}$  densities has been found.

PACS numbers: 21.10.Gv, 25.10.+s, 25.40.Cm, 25.60.Bx

## I. INTRODUCTION

As  $^{6,8}\text{He}$  beams with high energy resolution and intensity became available at different radioactive ion beam facilities around the world, these unstable helium isotopes are among the most studied light neutron-rich nuclei. Ever since the pioneering measurement of the interaction cross section in the late eighties [1, 2] which lead to the discovery of the extended density distribution of the valence halo neutrons in  $^{6,8}\text{He}$ , many recent experimental efforts are still focused on a more precise determination of the nuclear radii and radial shape of these nuclei by different methods [3]. The elastic proton scattering in inverse kinematics at energies around 700 MeV has been proven to be an accurate method to obtain information on the nuclear density distributions of the halo nuclei under study [4–7]. The first experiment on the (inverse kinematics) elastic proton scattering on  $^{6,8}\text{He}$  at energies around 700 MeV has been performed at GSI Darmstadt using the hydrogen-filled ionization chamber IKAR which simultaneously served as a gas target and a detector for the recoil protons [8], and the measured elastic scattering data were analyzed within the Glauber model [9] to deduce the matter radii and radial shape of the nuclear density distributions of these nuclei [10]. These same data were also studied in a Glauber few-body calculation of the elastic  $^{6,8}\text{He}+p$  scattering [11], where the few-body degrees of freedom were treated explicitly. We note that the first measurement [8] has covered only the region of low momentum transfer because the IKAR active target was limited to the detection of recoil ions close to  $\theta_{\text{lab}} \approx 90^\circ$ . Recently, a new experimental setup has been designed to study proton induced reactions on the exotic nuclei in inverse kinematics using a liquid hydrogen target adapted to obtain low-background data [12]. The new setup was successfully used to measure the elastic  $^{6,8}\text{He}+p$  scattering at energies around 700 MeV/nucleon, and the measured cross section has been extended to the region of higher momentum transfer as compared to the previous experiments. We note that the considered  $^{6,8}\text{He}+p$  data [8, 12] were originally deduced in terms of the scattering cross section versus the 4-momentum transfer squared ( $d\sigma/dt$ ). For a comparison between the results of different models, it is more convenient to use the elastic  $^{6,8}\text{He}+p$  scattering cross section versus the scattering angle ( $d\sigma/d\Omega$ ) in the center-of-momentum (c.m.) frame.

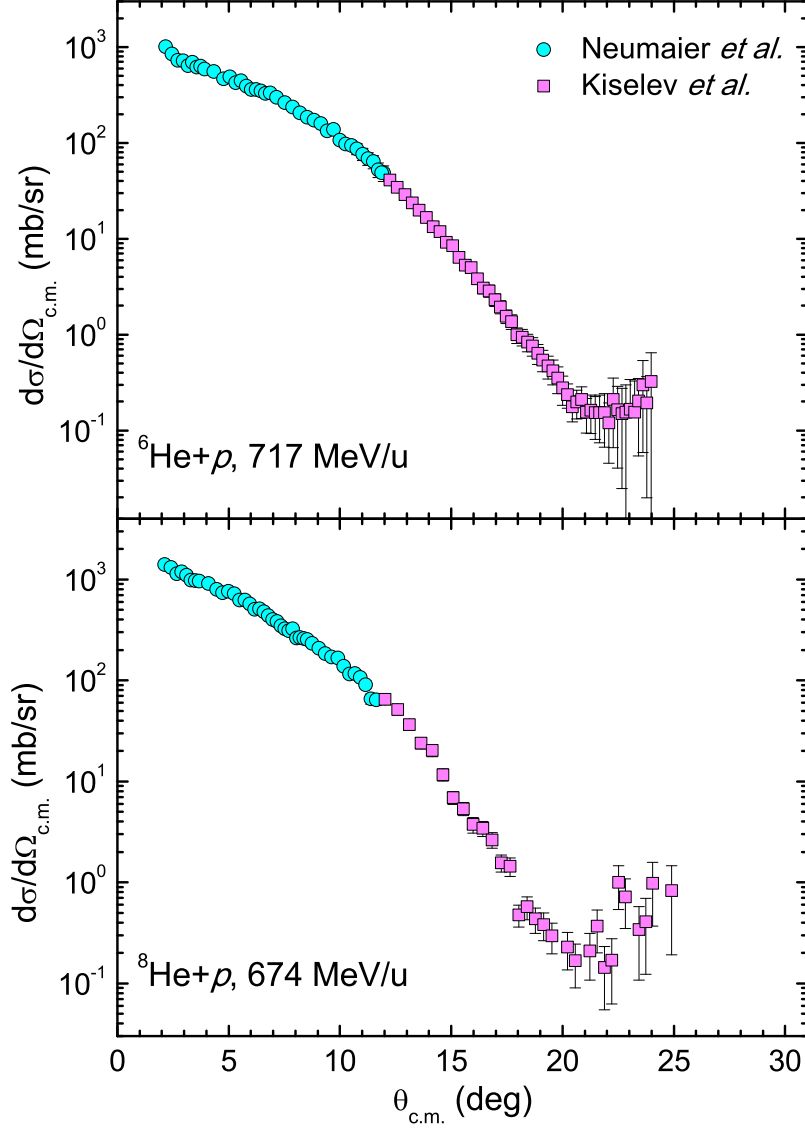


FIG. 1. (Color online) Elastic  ${}^{6,8}\text{He}+p$  scattering data at the energies around 700 MeV/nucleon measured by Neumaier *et al.* [8] and by Kiselev *et al.* [12] at the low and high momentum transfers, respectively.

The two cross sections are expressed through each other by the relativistic kinematics [13]

$$\begin{aligned} \cos \theta_{\text{c.m.}} &= 1 + \frac{t}{2k^2} \\ \Rightarrow \frac{d\sigma(\theta_{\text{c.m.}})}{d\Omega} &= \frac{k^2}{\pi} \frac{d\sigma(t)}{dt}. \end{aligned} \quad (1)$$

Here  $-t$  and  $k$  are the 4-momentum transfer squared and c.m. momentum, respectively. In terms of the scattering angles, the new data points measured at high momentum transfer [12] have reached the angular region around the first diffractive minimum (see Fig. 1), and

should be, therefore, more sensitive to the inner radial part of the ground-state densities of the  ${}^6,8\text{He}$  nuclei. The (first) diffractive minimum was observed at  $\theta_{\text{c.m.}} \approx 20^\circ \div 25^\circ$  in the  ${}^6\text{He}+p$  and  ${}^8\text{He}+p$  data taken at high momentum transfer.

In the present work, the elastic  ${}^6,8\text{He}+p$  scattering data under study have been analyzed within the Glauber multiple-scattering model (GMSM) using the same phenomenological parametrizations of the matter densities of  ${}^6,8\text{He}$  as those used in the earlier GMSM analyses of the GSI data [10]. Because the two measurements of Refs. [8, 12] were done practically at the same energy, it is possible to combine these two data sets in the present GMSM analysis.

## II. GLAUBER MULTIPLE-SCATTERING MODEL

The basic formalism of the GMSM has been given in details in Ref. [9]. The GMSM was successfully used in Refs. [4, 5, 10] to analyze the elastic  ${}^6,8\text{He}+p$  scattering data measured at low momentum transfer, and to deduce the nuclear matter density distributions for these nuclei. However, the GMSM calculations in Refs. [4, 10] were performed without taking into account the spin-orbital (s/o) interaction, because the s/o effects were known to be negligible at the most forward angles (low momentum transfer) [9]. Given the new data measured at high momentum transfer which cover the first diffractive minimum, the s/o effects should be significant and can no more be neglected (see, e.g., Fig. 23 of Ref. [9]). In the present work, the formalism of the GMSM that takes into account the s/o interaction has been used in the analysis of the new  ${}^6,8\text{He}+p$  data.

The proton-nucleus elastic scattering cross section is determined from the elastic scattering amplitude  $F_{\text{el}}$  as

$$\frac{d\sigma}{d\Omega_{\text{c.m.}}} = |F_{\text{el}}(\mathbf{q})|^2. \quad (2)$$

In general, the scattering amplitude can be written as [10, 14]

$$F_{\text{el}}(\mathbf{q}) = \frac{ik}{2\pi} \int e^{i\mathbf{q}\mathbf{b}} \left\{ 1 - \prod_{j=1}^A [1 - \gamma_{pN}(\mathbf{b} - \mathbf{s}_j)] \right\} \rho_A(\mathbf{r}_1, \mathbf{r}_2, \dots, \mathbf{r}_A) \prod_{j=1}^A d^3r_j d^2b. \quad (3)$$

For the light He nuclei, the effect of the center-of-mass motion should be significant. To effectively remove the spurious c.m. motion, the proton-nucleus scattering amplitude (3) is multiplied by a correction factor  $H_{\text{c.m.}}(\mathbf{q})$

$$H_{\text{c.m.}}(\mathbf{q}) = \exp \left[ \frac{\mathbf{q}^2 R_m^2}{6(A-1)} \right], \quad (4)$$

where  $R_m$  is the root-mean-square matter radius. Such a procedure is exact for the nucleon distributions of Gaussian form, and also expected to be accurate for the cases of non-Gaussian distributions [9].

Like the previous GSM studies [10], we have used in the present analysis several density models that divide explicitly the nuclear many-body density  $\rho_A(\mathbf{r}_1, \mathbf{r}_2, \dots, \mathbf{r}_A)$  into the core  $\rho_c(r)$  and halo  $\rho_h(r)$  parts, so that

$$\rho_A(\mathbf{r}_1, \mathbf{r}_2, \dots, \mathbf{r}_A) = \prod_{i=1}^4 \rho_{\text{core}}(r_i) \prod_{j=5}^A \rho_{\text{halo}}(r_j). \quad (5)$$

The representation (5) of the many-body density neglects the correlations between the nucleon locations, with a constraint that the positions of the core and halo nucleons are treated explicitly. In other cases, the nuclear many-body density has been simply assumed as a product of the one-body matter densities  $\rho_m(r)$

$$\rho_A(\mathbf{r}_1, \mathbf{r}_2, \dots, \mathbf{r}_A) = \prod_{j=1}^A \rho_m(r_j). \quad (6)$$

In the notations of Eq. (3),  $\mathbf{b}$  is the impact parameter,  $\mathbf{q}$  is the momentum transfer, and  $A$  is the nuclear mass number. The proton-nucleon ( $pN$ ) profile function  $\gamma_{pN}$  is determined from the amplitude  $f_{pN}$  of the free  $pN$  scattering as

$$\gamma_{pN}(\mathbf{b}) = \frac{1}{2\pi i k} \int \exp(-i\mathbf{q}\mathbf{b}) f_{pN}(\mathbf{q}) d^2q. \quad (7)$$

In difference from Refs. [8, 10], the present GSM calculation adopts the following parametrization of  $f_{pN}$  that takes into account also the s/o interaction

$$f_{pN}(\mathbf{q}) = f_{pN}^c(\mathbf{q}) + \boldsymbol{\sigma}(\hat{\mathbf{b}} \times \hat{\mathbf{k}}) f_{pN}^s(\mathbf{q}), \quad \text{with } \hat{\mathbf{b}} = \mathbf{b}/b, \quad \hat{\mathbf{k}} = \mathbf{k}/k. \quad (8)$$

Here,  $f_{pN}^c(\mathbf{q})$  and  $f_{pN}^s(\mathbf{q})$  are the central and s/o parts of the  $pN$  scattering amplitude,  $\boldsymbol{\sigma}$  is the Pauli spin operator. We have parametrized the  $f_{pN}^s$  amplitude in the same way as in Refs. [16, 17], taking into account explicitly the isotopic difference between the total neutron and proton cross sections. Thus, one has

$$\begin{aligned} f_{pN}^c(\mathbf{q}) &= \frac{k\sigma_{pN}}{4\pi} (\varepsilon_{pN} + i) \exp\left(-\frac{\mathbf{q}^2 \beta_{pN}}{2}\right), \quad N = p, n \\ f_{pN}^s(\mathbf{q}) &= \frac{k\sigma_{pN}}{4\pi} \sqrt{\frac{\mathbf{q}^2}{4M^2}} (i\alpha_s - 1) D_s \exp\left(-\frac{\mathbf{q}^2 \beta_s}{2}\right). \end{aligned} \quad (9)$$

Here  $\sigma_{pN}$  is the total  $pN$  cross section, parameters  $\varepsilon_{pN}$  and  $\alpha_s$  give the ratios of the real and imaginary strengths,  $\beta_{pN}$  and  $\beta_s$  are the slope parameters,  $D_s$  is the relative strength of the s/o amplitude, and  $M$  is the nucleon mass.

In the present work we have assumed the same parameters for the central amplitude  $f_{pN}^c$  as those used earlier in Ref. [10], except the slope parameters  $\beta_{pN}$  that were fine tuned to obtain the best description of the elastic  $p+{}^4\text{He}$  data at  $E_p \approx 700$  MeV [8, 15] in the GSM calculation that takes into account the s/o interaction explicitly. The reason is that the  $\beta_{pN}$  values used in Ref. [10] were adjusted to the best GSM description of the same  $p+{}^4\text{He}$  data without taking into account the s/o term. Thus,  $\beta_{pN}$  and parameters of the s/o term have been readjusted in the present work to the best description of the elastic  $p+{}^4\text{He}$  data at 700 MeV, as shown in Fig. 2. All the parameters used in the present GSM calculation are given in Table I, with the newly obtained  $\beta_{pN}$ ,  $D_s$ ,  $\beta_s$ , and  $\alpha_s$  values being quite close to those suggested earlier in Ref. [17]. The GSM results shown in Fig. 2 agree also with the

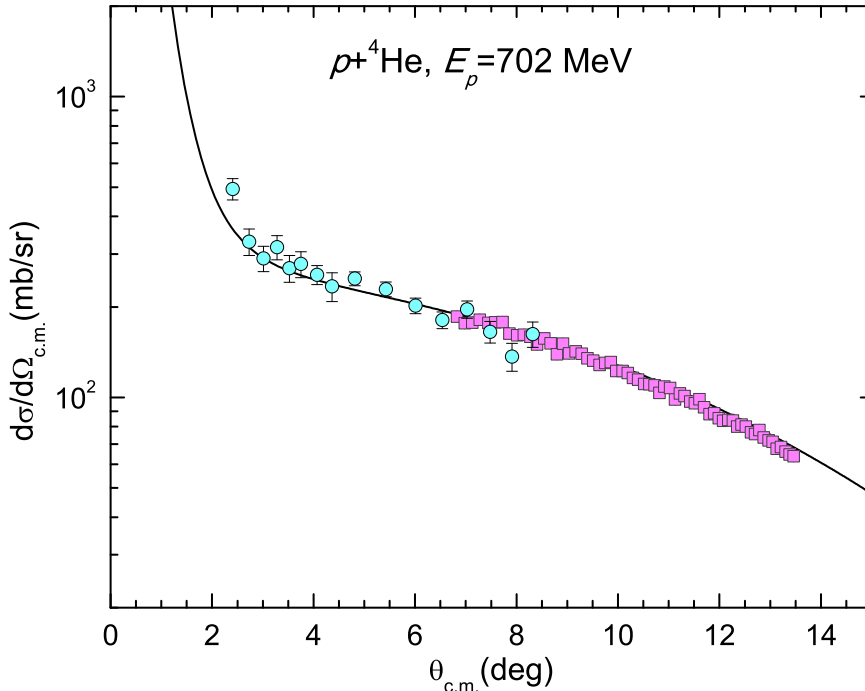


FIG. 2. (Color online) Elastic  $p+{}^4\text{He}$  scattering data measured at proton energies around 700 MeV (circles [8] and squares [15]) in comparison with the elastic scattering cross section given by the GSM calculation (solid line), taking into account the s/o term and using a Gaussian density for  ${}^4\text{He}$  that gives  $R_m = 1.47$  fm.

TABLE I. Parameters of the central and s/o scattering amplitudes (9) used in the present GMSM analysis of the elastic  ${}^6,8\text{He}+p$  scattering.

| System            | $E_p$<br>(MeV) | $\sigma_{pp}$<br>(mb) | $\varepsilon_{pp}$ | $\sigma_{pn}$<br>(mb) | $\varepsilon_{pn}$ | $\beta_{pp}$<br>(fm <sup>2</sup> ) | $\beta_{pn}$<br>(fm <sup>2</sup> ) | $D_s$ | $\alpha_s$ | $\beta_s$<br>(fm <sup>2</sup> ) |
|-------------------|----------------|-----------------------|--------------------|-----------------------|--------------------|------------------------------------|------------------------------------|-------|------------|---------------------------------|
| ${}^8\text{He}+p$ | 674            | 41.9                  | 0.129              | 37.4                  | -0.283             | 0.20                               | 0.24                               | 0.284 | 13.50      | 0.522                           |
| ${}^6\text{He}+p$ | 717            | 44.6                  | 0.069              | 37.7                  | -0.307             | 0.20                               | 0.24                               | 0.284 | 13.50      | 0.522                           |

fully quantal optical model results given by the complex  $p+{}^4\text{He}$  optical potential obtained from the folding model calculation [20] using the same Gaussian density for  ${}^4\text{He}$  and finite-range t-matrix interaction by Franey and Love [21]. This validates the parameters chosen for the present GMSM calculation.

Using the profile function  $\gamma_{pN}$  determined by the  $pN$  scattering amplitude (9) and treating the Coulomb term in the standard way [9, 14], the proton-nucleus elastic scattering amplitude can be written as [9, 18]

$$F_{\text{el}}^2(q) = |F_{\text{Coul}}(q) + F_c(q)|^2 + |F_s(q)|^2, \quad (10)$$

where  $F_c$  and  $F_s$  are the central and s/o proton-nucleus amplitudes [9, 18]

$$\begin{aligned} F_c(q) &= ikH_{\text{CM}}(q) \int [1 - G_c(b)] \exp[i\chi_{\text{Coul}}(b)] J_0(qb) b db, \\ F_s(q) &= -kH_{\text{CM}}(q) \int G_s(b) \exp[i\chi_{\text{Coul}}(b)] J_1(qb) b db. \end{aligned} \quad (11)$$

The  $G$  functions contain explicitly the central and s/o contributions as

$$\begin{aligned} G_c(b) &= \frac{1}{2} \left\{ \prod_{j=1}^A [1 - \Gamma_j^c(b) + \Gamma_j^s(b)] + \prod_{j=1}^A [1 - \Gamma_j^c(b) - \Gamma_j^s(b)] \right\}, \\ G_s(b) &= \frac{1}{2} \left\{ \prod_{j=1}^A [1 - \Gamma_j^c(b) + \Gamma_j^s(b)] - \prod_{j=1}^A [1 - \Gamma_j^c(b) - \Gamma_j^s(b)] \right\}. \end{aligned} \quad (12)$$

The nucleon profile functions  $\Gamma^c$  and  $\Gamma^s$  are determined as

$$\begin{aligned} \Gamma_j^c(b) &= -\frac{i}{k} \int f_{pN}^c(q) S_j(q) J_0(qb) q dq, \\ \Gamma_j^s(b) &= -\frac{1}{k} \int f_{pN}^s(q) S_j(q) J_1(qb) q dq. \end{aligned} \quad (13)$$

Here  $J_{0,1}(x)$  are the zero-th and first-order Bessel functions.  $F_{\text{Coul}}(q)$  and  $\chi_{\text{Coul}}(b)$  are the Coulomb amplitude and phase, respectively [14]. In difference from the earlier GMSM

calculations [6, 7, 10], the Sommerfeld parameter (used to determine the Coulomb term) obtained with the relativistic kinematics has been used in the present work. The form factor  $S_j(q)$  is determined by the Fourier transform of the single-particle density as

$$S_j(q) = \frac{1}{H_{\text{CM}}(q)} \int \exp(i\mathbf{q}\mathbf{r})\rho_j(r)d^3r. \quad (14)$$

When one writes explicitly the products in Eq. (12) in terms of the nucleon profile functions, the proton-nucleus scattering amplitude becomes a multiple scattering series [9]. When the s/o term is neglected, the amplitude (10) is simplified to that used in the earlier GSM calculation that did not take into account the s/o interaction [6, 7, 10].

### III. NUCLEAR DENSITIES

#### A. Parametrization of the nuclear matter distribution

In addition to the proton-nucleon scattering amplitudes, the nuclear matter density distribution is a vital input of the Glauber model calculation. Like in the previous studies [10, 14], the nucleon point-density has been parametrized in the following phenomenological forms.

##### 1. The symmetrized Fermi (SF) density

The SF density distribution is parametrized [10] as

$$\rho_m(r) = \frac{3}{4\pi R_0^3} \left[ 4 + \left( \frac{\pi a}{R_0} \right)^2 \right]^{-1} \sinh \left( \frac{R_0}{a} \right) \left[ \cosh \left( \frac{R_0}{a} \right) + \cosh \left( \frac{r}{a} \right) \right]^{-1}, \quad (15)$$

where  $R_0$  is the half-density radius (at which the density becomes twice smaller than at the origin) and  $a$  is the diffuseness parameter. The corresponding root-mean-square (rms) matter radius  $R_m$  is given by

$$R_m = \langle r^2 \rangle^{1/2} = \left( \frac{3}{5} \right)^{1/2} R_0 \left[ 1 + \frac{7}{3} \left( \frac{\pi a}{R_0} \right)^2 \right]^{1/2}. \quad (16)$$



## 2. The Gaussian-Halo (GH) density

The GH density distribution is determined [10] as a function of the rms radius  $R_m$  as

$$\rho_m(r) = \left( \frac{3}{2\pi R_m^2} \right)^{3/2} [1 + \alpha\varphi(r)] \exp\left(-\frac{3r^2}{2R_m^2}\right) \quad (17)$$

with

$$\varphi(r) = \frac{3}{4} \left[ 5 - 10 \left( \frac{r}{R_m} \right)^2 + 3 \left( \frac{r}{R_m} \right)^4 \right]. \quad (18)$$

## 3. The Woods-Saxon (WS) density

The WS density has been used by Glauber in his pioneering work [14]

$$\rho_m(r) = \frac{C}{1 + \exp\left(\frac{r - R_0}{a}\right)}, \quad (19)$$

where  $R_0$  and  $a$  are the same parameters as those used in Eq. (15), and  $C$  is normalized such that (19) is the nucleon point-density.

## 4. The Gaussian-Gaussian (GG) density

In the GG parametrization the locations of the core and halo nucleons are treated explicitly, with both the core and halo densities assumed to be in the Gaussian form [10]

$$\rho_{\text{core(halo)}}(r) = \left( \frac{3}{2\pi R_{\text{c(h)}}^2} \right)^{3/2} \exp\left(-\frac{3r^2}{2R_{\text{c(h)}}^2}\right). \quad (20)$$

## 5. The Gaussian-Oscillator (GO) density

The GO density has the same Gaussian core as in the GG case, but the halo distribution is parametrized using the  $p$ -shell harmonic oscillator wave function [10]

$$\begin{aligned} \rho_{\text{core}}(r) &= \left( \frac{3}{2\pi R_c^2} \right)^{3/2} \exp\left(-\frac{3r^2}{2R_c^2}\right) \\ \rho_{\text{halo}}(r) &= \frac{5}{3} \left( \frac{5}{2\pi R_h^2} \right)^{3/2} \left( \frac{r}{R_h} \right)^2 \exp\left(-\frac{5r^2}{2R_h^2}\right). \end{aligned} \quad (21)$$

Because the GG and GO models allow to treat the core and halo nucleons explicitly, the nuclear volumes of  ${}^6\text{He}$  and  ${}^8\text{He}$  can be assumed to be composed of an  $\alpha$ -like core plus 2

and 4 halo neutrons, respectively. The nuclear many-body density based on the GG and GO parametrizations can be expressed as (5). We can further write

$$\rho_{\text{m}}(r) = [N_{\text{core}}\rho_{\text{core}}(r) + N_{\text{halo}}\rho_{\text{halo}}(r)]/A, \quad (22)$$

where  $\rho_{\text{core(halo)}}$  are normalized to unity like  $\rho_{\text{m}}$ , and  $N_{\text{core}}$  and  $N_{\text{halo}}$  are the nucleon numbers in the core and halo volumes, respectively. From Eq. (22) one obtains the rms matter radius of the nucleus as

$$R_{\text{m}} = \left[ \int r^2 \rho_{\text{m}}(r) d^3r \right]^{1/2}. \quad (23)$$

The core and halo radii ( $R_{\text{c}}$  and  $R_{\text{h}}$ ) are determined by the same Eq. (23) using  $\rho_{\text{core}}$  and  $\rho_{\text{halo}}$ , respectively.

### B. $\chi^2$ -fit procedure for the density parameters

Each phenomenological density distribution determined above has two free parameters (like  $R_0$  and  $a$  in the SF and WS parametrizations). The aim of the present analysis is to find the optimal values of these parameters based on the best GSM description of the experimental data. In the  $\chi^2$ -fit procedure, the density parameters are varied independently from each other, and the statistical errors as well as the uncertainty in the absolute normalization of the measured scattering cross sections are taken properly into account [10].

The elastic scattering cross sections at the low and high momentum transfers were measured at practically the same energy, and this allows us to combine both data sets in the present analysis. Thus, the  $\chi^2$  function is determined as

$$\begin{aligned} \chi^2 = & \sum_{j=1}^{N_L} \left[ \frac{A_L \sigma_{\text{exp}}(\theta_j) - \sigma_{\text{cal}}(\theta_j)}{\Delta \sigma_{\text{exp}}(\theta_j)} \right]^2 + \sum_{k=1}^{N_H} \left[ \frac{A_H \sigma_{\text{exp}}(\theta_k) - \sigma_{\text{cal}}(\theta_k)}{\Delta \sigma_{\text{exp}}(\theta_k)} \right]^2 \\ & + \left( \frac{A_L - 1}{\Delta A_{\text{exp}}^L} \right)^2 + \left( \frac{A_H - 1}{\Delta A_{\text{exp}}^H} \right)^2, \end{aligned} \quad (24)$$

where  $\sigma_{\text{exp}}(\theta_j) \equiv [d\sigma/d\Omega_{\text{c.m.}}(\theta_j)]_{\text{exp}}$  and  $\Delta \sigma_{\text{exp}}(\theta_j)$  are the experimental differential cross sections measured at  $\theta_j$  and their statistical errors, and  $\sigma_{\text{cal}}(\theta_j) \equiv [d\sigma/d\Omega_{\text{c.m.}}(\theta_j)]_{\text{cal}}$  are the calculated cross sections.  $N_L$  and  $N_H$  are the number of data points measured at low [8] and high momentum transfers [12], respectively.  $A_L$  and  $A_H$  are the absolute normalization of the data points at low and high momentum transfers, and they are treated as free parameters in the  $\chi^2$ -fit, with the estimated uncertainties of the absolute calibration  $\Delta A_{\text{exp}}^L \approx 3\%$  [8] and  $\Delta A_{\text{exp}}^H \approx 2.4\%$  [12].

## IV. RESULTS OF THE GSM ANALYSIS AND DISCUSSION

### A. The matter radii and matter distributions of ${}^{6,8}\text{He}$

The  $\chi^2$  analysis has been done carefully for each density parametrization to obtain the best GSM description of the elastic  ${}^6\text{He}$  and  ${}^8\text{He}$  scattering data measured at the energies of 717 and 674 MeV/u, respectively. All the best-fit parameters are presented in Tables II and III. The elastic  ${}^{6,8}\text{He}+p$  scattering cross sections given by the GSM calculation using the best-fit parameters (see Tables II and III) of the nuclear matter densities are compared with the data in Figs. 3 and 4. Focusing on the new data points measured at high momentum transfer, one can see that the first diffraction maximum in the elastic scattering cross section is now fully covered by the data and it turned out that the combined data set allowed for an improved determination of the parameters of the density distribution. The data and the calculated cross sections divided by the Rutherford cross section are presented in Figs. 3 and 4, and one can see that the elastic  ${}^{6,8}\text{He}+p$  scattering at the considered energies is strongly dominated by the nuclear scattering, and that allows the fine-tuning of the density inputs

TABLE II. The best-fit parameters of the nuclear densities (15)-(21) obtained from the present GSM analysis of the combined set of the elastic  ${}^6\text{He}+p$  scattering data measured at low [8] and high momentum transfer [12]. The relative  $\chi_r^2$  is per data point, and the errors are statistical. The neutron radius  $R_n$  is determined with the assumption that the proton and core radii are the same, i.e.,  $R_p = R_c$ . The COSMA density (25) is parametrized by the same functional as that of the GO density model, with the corresponding parameters given in round brackets.

| density | $A_L$   | $A_H$   | density parameters      |                         | $R_m$<br>(fm) | $\chi_r^2$ | $R_n$<br>(fm) | $R_n - R_p$<br>(fm) |
|---------|---------|---------|-------------------------|-------------------------|---------------|------------|---------------|---------------------|
|         |         |         | (fm)                    | (fm)                    |               |            |               |                     |
| GG      | 1.04(3) | 1.09(4) | $R_c=1.96(4)$           | $R_h=3.30(12)$          | 2.48(6)       | 1.41       | 2.71(7)       | 0.75(8)             |
| GO      | 1.05(2) | 1.04(2) | $R_c=1.90(3)$           | $R_h=3.26(13)$          | 2.44(5)       | 0.88       | 2.67(8)       | 0.77(9)             |
| GH      | 1.04(3) | 1.09(3) | $R_m=2.45(4)$           | $\alpha=0.12(2)$        | 2.45(4)       | 1.39       |               |                     |
| SF      | 1.05(4) | 1.09(3) | $R_0=1.00(8)$           | $a=0.61(2)$             | 2.40(5)       | 1.55       |               |                     |
| WS      | 1.04(2) | 1.07(3) | $R=0.99(5)$             | $a=0.63(2)$             | 2.45(6)       | 1.00       |               |                     |
| COSMA   | 1.00    | 1.00    | $a=1.55$ ( $R_c=1.90$ ) | $b=2.12$ ( $R_h=3.35$ ) | 2.48          | 1.49       | 2.72          | 0.82                |

for the GSM calculation by the  $\chi^2$ -fit procedure (24).

From a comparison of the best-fit matter radii  $R_m$  obtained in the present work for  ${}^6,8\text{He}$  with the results of the earlier GSM analysis [10] based on the low-momentum data only [8], we found that the newly obtained  $R_m$  values are slightly larger than those reported in Ref. [10]. In terms of the  $\chi^2$ -fit, the accuracy of the present GSM analysis is about the same as that of Ref. [10]. The nuclear radii obtained in the present work are also in a sound agreement with the empirical matter radii of  ${}^6,8\text{He}$  discussed recently by Tanihata *et al.* in Ref. [3]. The GG and GO density models treat the core and halo parts explicitly, and we could determine from our GSM analysis the neutron skin of 0.76(10) and 0.94(13) fm for  ${}^6\text{He}$  and  ${}^8\text{He}$ , respectively. Such neutron skins are much thicker than, e.g., the neutron skin of around 0.2  $\sim$  0.3 fm established for the heavy  ${}^{208}\text{Pb}$  nucleus with a large neutron excess, and clearly associated with the halo structure of the  ${}^6\text{He}$  and  ${}^8\text{He}$  isotopes. It is noteworthy that both the GG and GO density models give the best-fit core radius for  ${}^6\text{He}$  slightly larger than that for  ${}^8\text{He}$ , and that makes the difference in the observed neutron skin because the neutron radii are about the same for the two nuclei. Such an effect was also found in the earlier GSM analysis of the elastic  ${}^6,8\text{He}+p$  scattering data taken at low-momentum transfer [10], and it might be due to different polarizing contributions of the valence neutrons to the motion of the  $\alpha$ -core. Quite complementary to this discussion are the high-precision laser spectroscopy data that yield a charge radius of 2.068(11) fm for  ${}^6\text{He}$ , which is significantly larger than the charge radius of 1.93(3) fm obtained for  ${}^8\text{He}$  [22].

TABLE III. The same as table II but for the  ${}^8\text{He}+p$  system

| density | $A_L$   | $A_H$   | density parameters      |                         | $R_m$<br>(fm) | $\chi_r^2$ | $R_n$<br>(fm) | $R_n - R_p$<br>(fm) |
|---------|---------|---------|-------------------------|-------------------------|---------------|------------|---------------|---------------------|
|         |         |         | (fm)                    | (fm)                    |               |            |               |                     |
| GG      | 1.00(2) | 0.99(6) | $R_c=1.81(6)$           | $R_h=3.12(13)$          | 2.55(8)       | 1.35       | 2.75(10)      | 0.94(12)            |
| GO      | 1.03(2) | 0.95(7) | $R_c=1.69(6)$           | $R_h=2.99(14)$          | 2.43(9)       | 1.50       | 2.63(11)      | 0.94(12)            |
| GH      | 1.01(2) | 0.98(6) | $R_m=2.50(5)$           | $\alpha=0.13(4)$        | 2.50(5)       | 1.35       |               |                     |
| SF      | 1.01(2) | 0.96(5) | $R_0=0.66(4)$           | $a=0.66(2)$             | 2.51(7)       | 1.16       |               |                     |
| WS      | 1.01(2) | 0.97(5) | $R=0.80(8)$             | $a=0.66(2)$             | 2.51(5)       | 1.15       |               |                     |
| COSMA   | 1.00    | 1.00    | $a=1.38$ ( $R_c=1.69$ ) | $b=1.99$ ( $R_h=3.15$ ) | 2.53          | 2.15       | 2.75          | 1.06                |

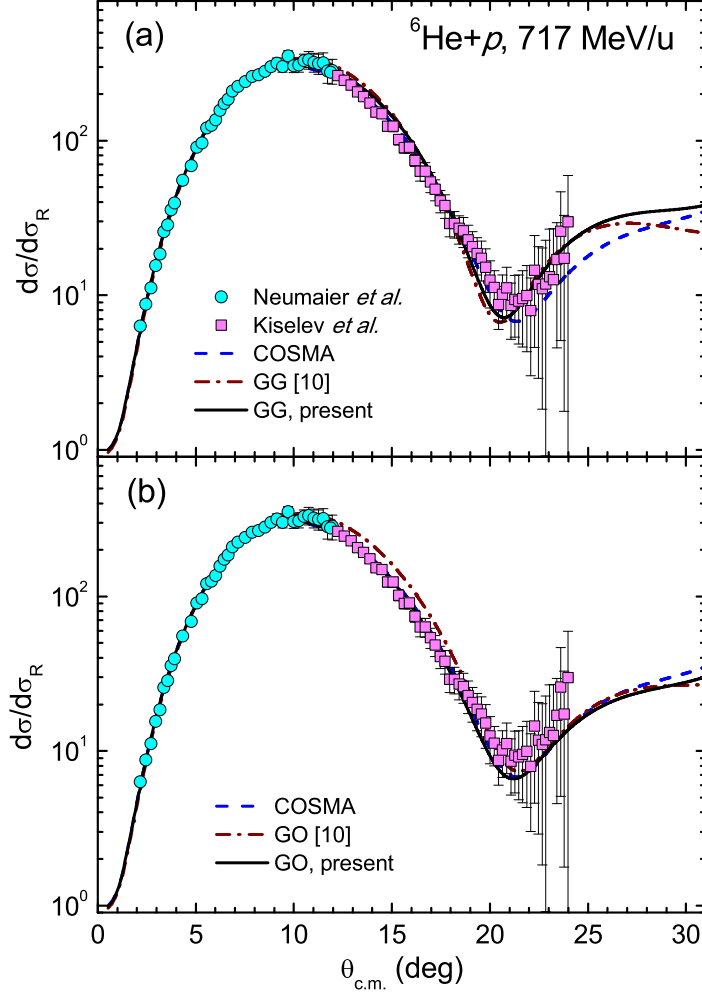


FIG. 3. (Color online) Elastic  ${}^6\text{He}+p$  scattering cross sections (divided by Rutherford cross section) obtained with the GMSM calculation (solid curve) using the best-fit parameters of the GG (a) and GO (b) models of the nuclear density, in comparison with the data measured by Neumaier *et al.* [8] and by Kiselev *et al.* [12] at low and high momentum transfers, respectively. The dash-dotted curves were obtained with the best-fit parameters of the GG and GO density models taken from Ref. [10], and the dashed curves were obtained with the  ${}^6\text{He}$  density given by the cluster-orbital shell-model approximation (COSMA) [23].

After the standard correction for the finite size of the proton [3], we can obtain the proton radii of 1.925(12) and 1.81(3) fm for  ${}^6\text{He}$  and  ${}^8\text{He}$ , respectively, from the laser spectroscopy data. Such proton radii are in a good agreement with the core radii of  ${}^6\text{He}$  and  ${}^8\text{He}$  given by the present GMSM analysis (see  $R_c$  values in Tables II and III).

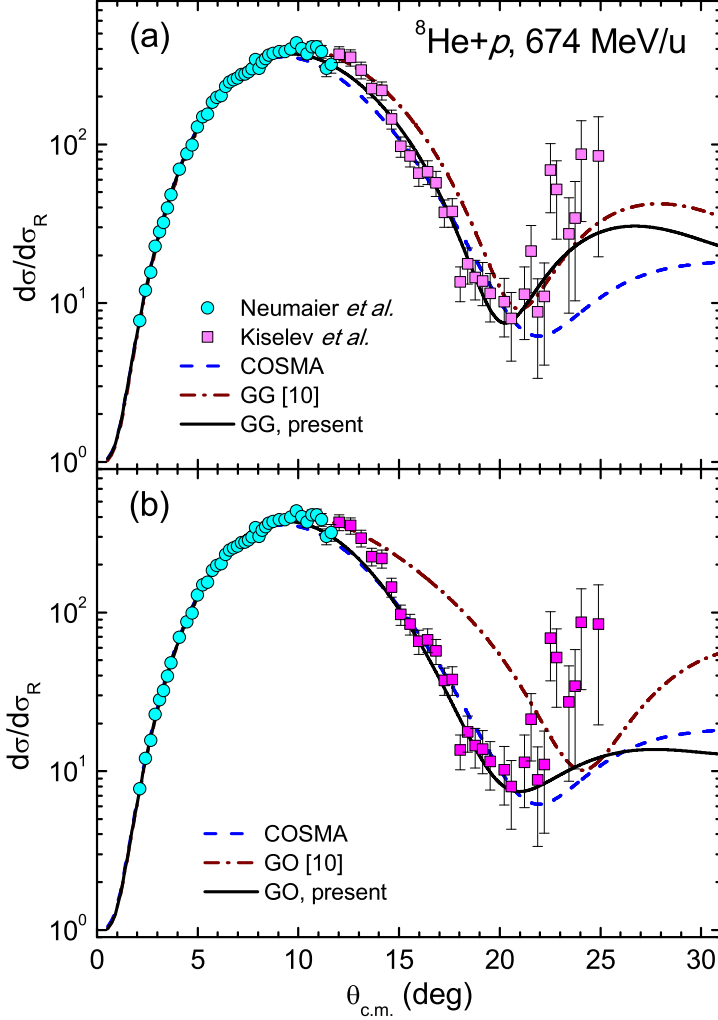


FIG. 4. (Color online) The same as Fig. 3 but for the  ${}^8\text{He}+p$  scattering.

To compare with the available results for the microscopic nuclear densities predicted by the cluster-orbital shell-model approximation (COSMA) [23], we have also used the COSMA densities as input for the present GSM calculation, and the results are presented in Tables II and III and Figs. 3 and 4. One can see that the COSMA densities give a good description of the  ${}^6\text{He}+p$  data, but fail to account for the data points taken at angles beyond the diffractive minimum for the  ${}^8\text{He}+p$  system. Because the newly measured data points at large angles allowed us to improve the density parameters of the density models, these data are also helpful in fine-tuning the existing parameters of the COSMA density [23]. Namely, from the explicit expression of the COSMA density

$$\rho_m(r) = N_{\text{core}} \frac{\exp(-r^2/a^2)}{\pi^{3/2}a^3} + N_{\text{halo}} \frac{2 \exp(-r^2/b^2)}{3\pi^{3/2}b^5} r^2, \quad (25)$$

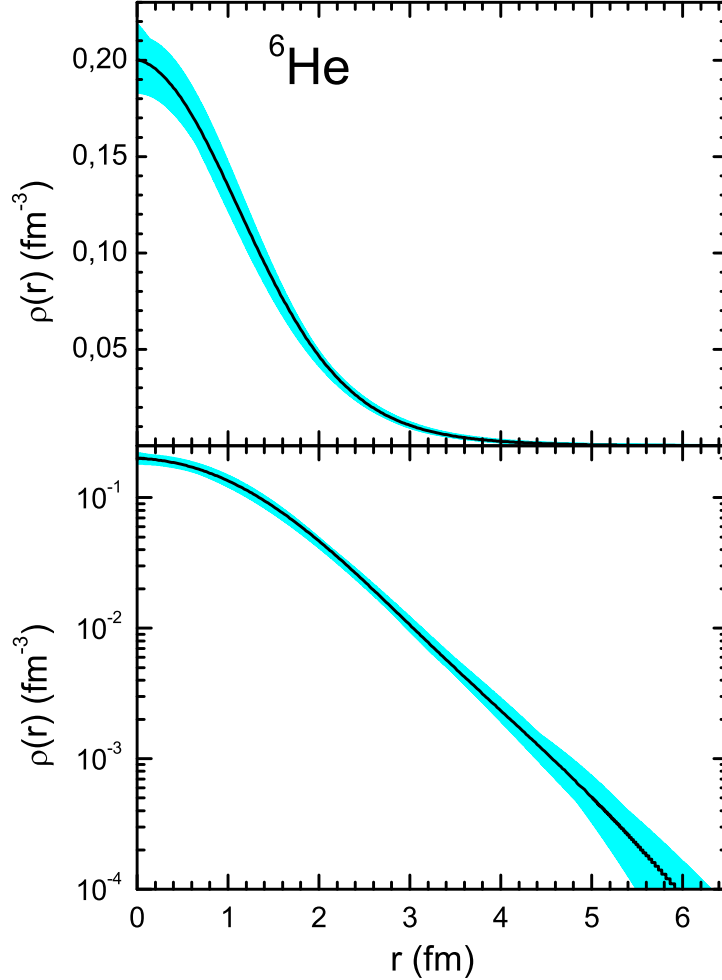


FIG. 5. (Color online) The average nuclear matter density distribution of  ${}^6\text{He}$  (upper panel) deduced from the GSM fit to the data using the present SF, GH, WS, GG and GO parametrizations, with the uncertainty band determined by the statistical errors of the best-fit parameters of the density models. The same density is plotted in logarithmic scale in the lower panel to illustrate the uncertainty at large radii.

we find immediately from the best-fit parameters of the GO model in Tables II and III that the improved  $a$  and  $b$  parameters of COSMA are 1.55(2) and 2.06(8) fm, respectively, for  ${}^6\text{He}$ , and 1.38(5) and 1.89(9) fm for  ${}^8\text{He}$ .

With the new parameters of the considered density models given in Tables II and II, it is of interest to construct the average radial shape of the nuclear matter density distributions for the  ${}^6\text{He}$  and  ${}^8\text{He}$  isotopes. The radial profiles of the nuclear matter densities of the  ${}^6\text{He}$  and  ${}^8\text{He}$  isotopes based on the best-fit parameters of 5 density models are plotted in

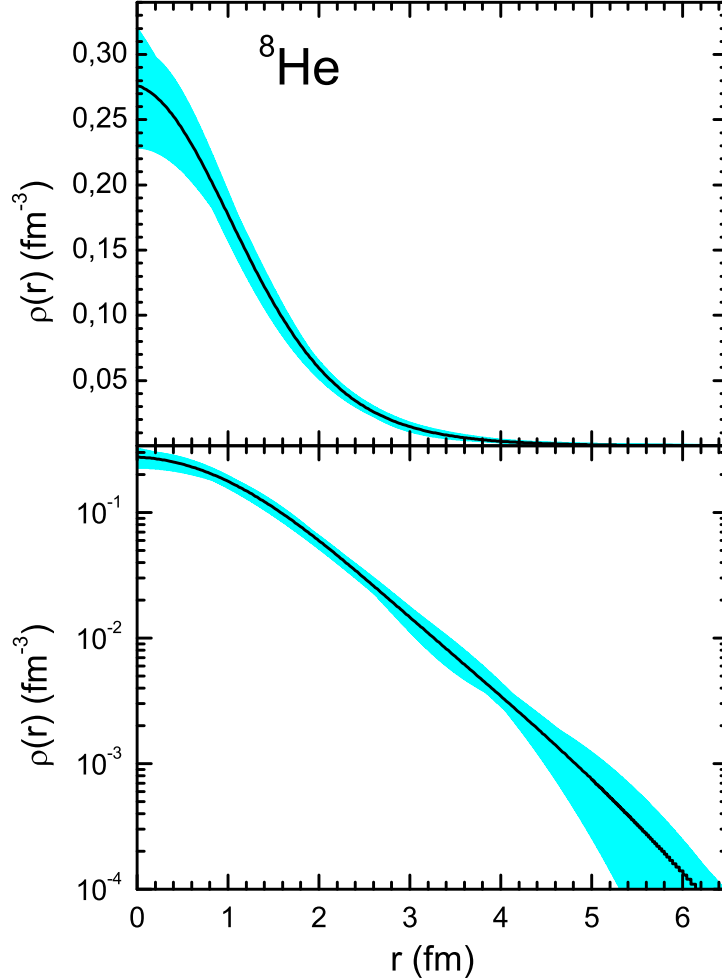


FIG. 6. (Color online) The same as Fig. 5 but for the matter distribution of  ${}^8\text{He}$ .

Figs. 5 and 6, respectively. The errors in tables II and III are statistical errors coming from fitting and data point normalization. The total errors should have included, in addition, the contribution from the uncertainties in the  $pN$  scattering amplitudes, the  $t$ -scale calibration, and model uncertainty [10]. Thus, the final averaged nuclear matter radii  $R_m$  of the  ${}^6\text{He}$  and  ${}^8\text{He}$  isotopes obtained from the consistent GSM analysis using the five phenomenological parametrizations of nuclear matter density are

$$R_m = 2.44 \pm 0.07 \text{ fm for } {}^6\text{He},$$

$$R_m = 2.50 \pm 0.08 \text{ fm for } {}^8\text{He}.$$

We note further, in connection with the realistic core (or proton) radii of the  ${}^6\text{He}$  and  ${}^8\text{He}$  nuclei discussed above, the results of the Glauber few-body calculation [11] of the elastic  ${}^6,8\text{He}+p$  scattering that gives a very nice description of the data measured at low transfer



momentum, using the microscopic few-body model that gives the nuclear matter radii of the  ${}^6\text{He}$  and  ${}^8\text{He}$  nuclei  $R_m \approx 2.50$  and  $2.60$  fm, respectively. These values are somewhat larger than those obtained in Ref. [10] (based on the data measured at low transfer momentum) and in the present work (based on the complete data set extended to high transfer momentum). A likely reason for such a disagreement is the assumption of the rigid  $\alpha$ -core of the fixed radius  $R_c \approx 1.49$  fm in the few-body calculation, which is not the case in view of the high-precision laser spectroscopy data [22] that give the proton radii of  $1.925(12)$  and  $1.81(3)$  fm for  ${}^6\text{He}$  and  ${}^8\text{He}$ , respectively. Such an effect is expected to be due to the different polarizing contributions of the valence neutrons to the motion of the  $\alpha$ -core in these two nuclei [3]. It is, therefore, of high interest to have the few-body calculation [11] redone using the quoted experimental values for the  $\alpha$ -core radius.

### **B. Sensitivity of the data to the core and halo parts of the matter distribution, and to the spin-orbit term**

Taking into account the new data taken at high momentum transfer, it is naturally to expect that these data points are more sensitive to the inner part of the density distribution compared to the sensitivity of the data taken at low momentum transfer only. We have made, therefore, some comparisons of the GSM results obtained for the  ${}^8\text{He}+p$  case with the halo or core radius of the GG or GO density model fixed, and the other radius (core or halo) being changed up and down by about 0.1 fm from the best-fit values given in Table III. From the GSM results shown in the upper panel of Fig. 7 one can see that the data measured at high momentum transfer are indeed sensitive to the core part of the density distribution of  ${}^8\text{He}$ . A similar variation of the halo radius resulted on a much smaller change in the calculated elastic scattering cross section that is hardly visible in the logarithmic scale (lower panel of Fig. 7). Similar results were also found for the  ${}^6\text{He}+p$  case, and these results confirm that the elastic scattering data measured at high momentum transfer are very valuable for a precise determination of the core matter density of a halo nucleus. Note that the GG and GO density parametrizations are defined with an assumption that both the  ${}^6\text{He}$  and  ${}^8\text{He}$  nuclei have a  $\alpha$ -like core. The present GSM analysis using the GG and GO density parametrizations has reached a good fit of the data (see  $\chi^2$  values in Tables II and III) and we obtained the following average core and halo radii of the two He isotopes

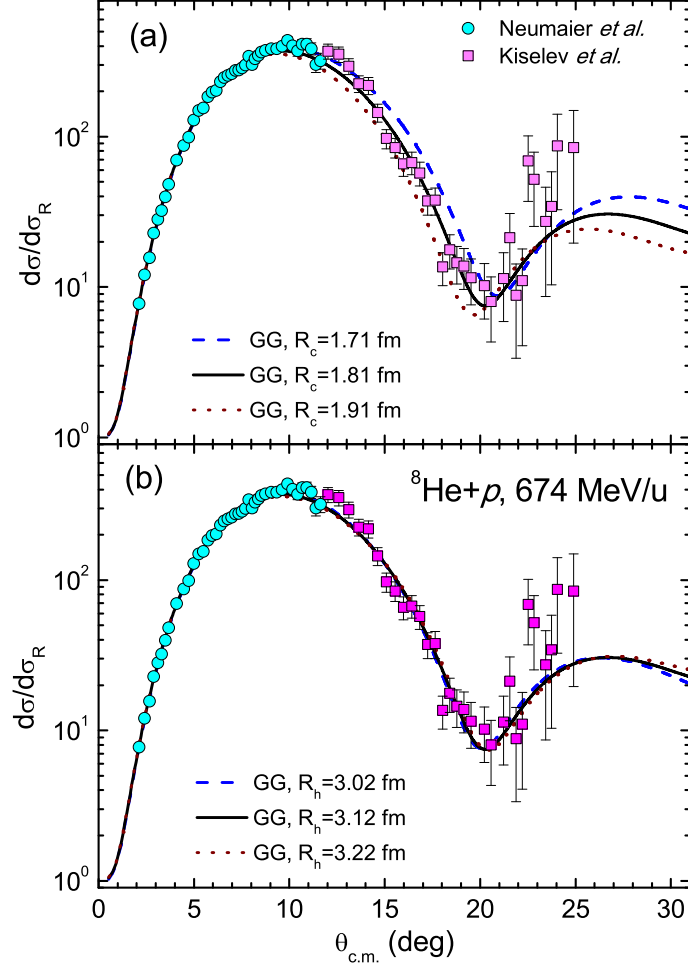


FIG. 7. (Color online) The sensitivity of the elastic  ${}^8\text{He}+p$  data to the core (a) and halo (b) parts of the GG density of  ${}^8\text{He}$  being used in the GSM calculation. See text for more details.

$$\begin{aligned}
 R_c &= 1.93 \pm 0.06 \text{ fm}, \quad R_h = 3.28 \pm 0.13 \text{ fm} \text{ for } {}^6\text{He}, \\
 R_c &= 1.75 \pm 0.08 \text{ fm}, \quad R_h = 3.06 \pm 0.14 \text{ fm} \text{ for } {}^8\text{He}.
 \end{aligned}$$

As discussed above, the  $\alpha$ -core radius of  ${}^6\text{He}$  is slightly larger than that of  ${}^8\text{He}$ , and the  $R_c$  values are quite close to the proton radii of  ${}^6\text{He}$  and  ${}^8\text{He}$  deduced from the laser spectroscopy data. This is a clear indication of the different polarizing contributions of the valence neutrons to the motion of the  $\alpha$ -core in the  ${}^{6,8}\text{He}$  nuclei.

We note further that the inclusion of the spin-orbit amplitude into the GSM calculation is necessary for the analysis of the elastic data measured at large scattering angles or high momentum transfer. The GSM results plotted in Fig. 8 show clearly the important contribution of the s/o term around the first diffractive minimum as discussed earlier by Alkhozov

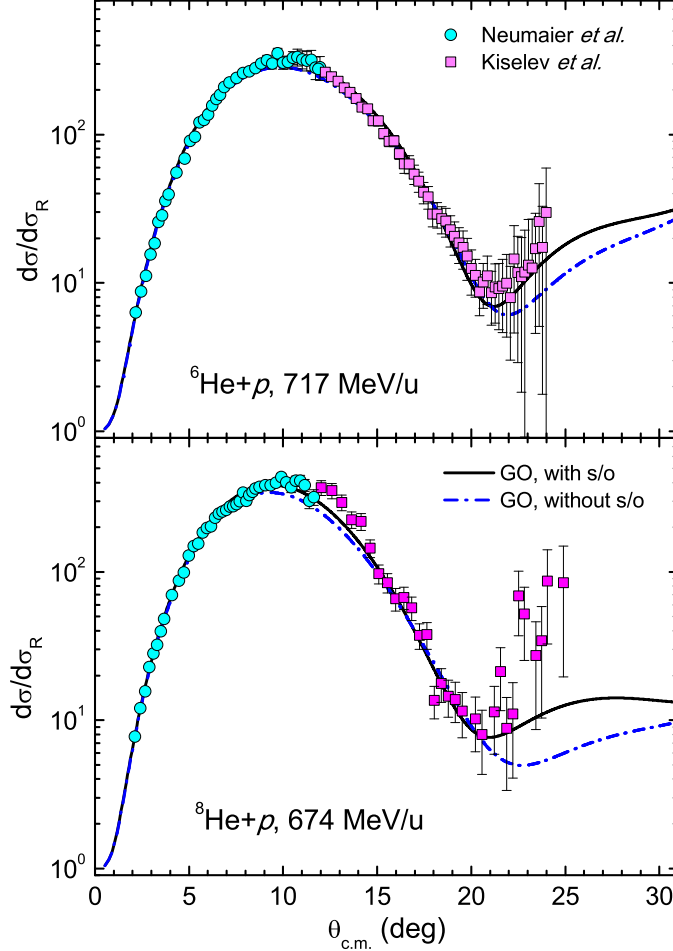


FIG. 8. (Color online) Results of the GSM calculation of the elastic  $^{6,8}\text{He}+p$  scattering using the GO density models, with or without the inclusion of the spin-orbit term.

[9]. The full GSM calculation with both the central and s/o amplitudes included also resulted on slightly larger matter radii for  $^{6,8}\text{He}$  nuclei, which are closed to the empirical values [3].

### C. Nuclear geometry for the 2-neutron halo in the $^6\text{He}$ nucleus

In this section, we apply our GSM results to the 2-neutron halo geometry like that used by Tanihata *et al.* in Ref. [3] for  $^6\text{He}$ . In this model, the core is assumed to be a free core nucleus that moves around the nuclear center of mass, like the 2-neutron halo does. As a result, the size of the effective core is bigger than the free  $\alpha$ -particle, and the extended matter distribution is mainly determined by the location of the 2-neutron halo.

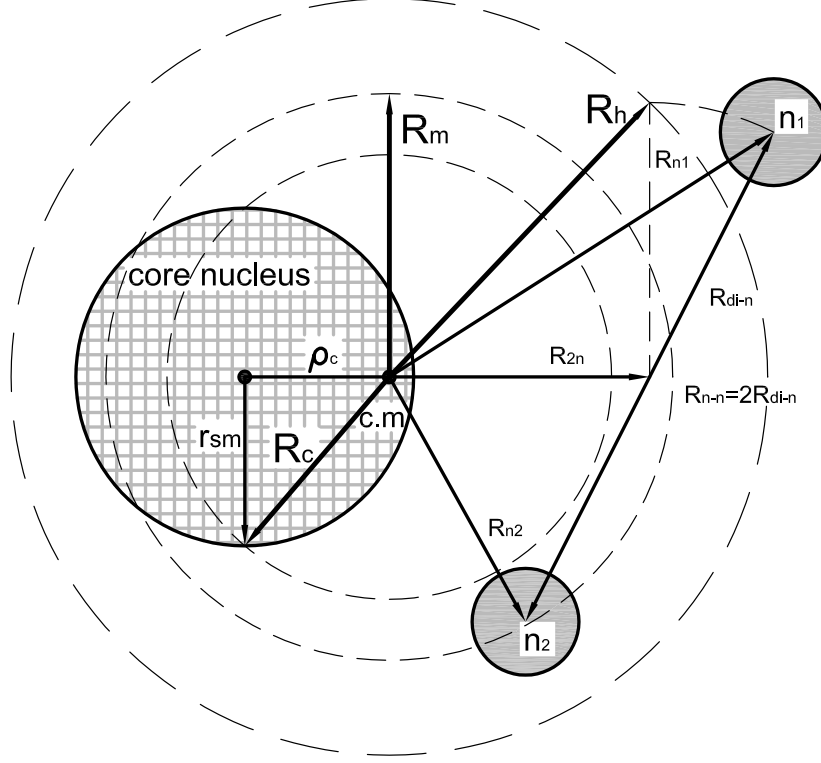


FIG. 9. The nuclear geometry for a 2-neutron halo nucleus. See text for more details

The geometrical model of the Borromean  ${}^6\text{He}$  nucleus is shown in Fig. 9, where the nuclear radii under discussion are defined.

Because the core is an  $\alpha$ -cluster, the matter, proton and neutron radii of the core nucleus can be assumed equal  $r_{sm} = r_{sp} = r_{sn} = 1.46$  fm [3]. Using these values and  $R_m$ ,  $R_c$ ,  $R_h$ ,  $R_n$  radii given by the present GSM analysis with the GG and GO density models, the radii of the geometry shown in Fig. 9 can be determined [3] as.

- The distance  $\rho_c$  between the nuclear center of mass and the core center is

$$\rho_c = \sqrt{R_c^2 - r_{sm}^2}. \quad (26)$$

- The vector  $R_{2n}$  joining the nuclear center of mass and the midpoint of the line connecting the two halo neutrons is determined from the balancing condition

$$A_c \rho_c = A_h R_{2n}, \text{ where } A_c = 4, A_h = 2. \quad (27)$$

- The distance  $R_{c-2n}$  from the core center to the two halo neutrons is

$$R_{c-2n} = \rho_c + R_{2n}. \quad (28)$$

TABLE IV. The radii (in fm) of the geometrical model [3] for the 2-neutron halo nucleus  ${}^6\text{He}$  in comparison with the results of the present work.

| ${}^6\text{He}$                       | Definition from Ref. [3]          | Present work | Ref. [3]  |
|---------------------------------------|-----------------------------------|--------------|-----------|
| $R_m$                                 | $R_m$                             | 2.44(7)      | 2.43(3)   |
| $R_p$                                 | $R_c$                             | 1.93(6)      | 1.912(18) |
| $R_h$                                 | $R_h$                             | 3.28(13)     | 3.37(11)  |
| $R_n$                                 | $R_n$                             | 2.69(9)      | 2.65(4)   |
| $R_n - R_p$                           | $R_n - R_p$                       | 0.76(10)     | 0.808(47) |
| $\rho_c$                              | $(R_c^2 - r_{\text{sm}}^2)^{1/2}$ | 1.26(7)      |           |
| $R_{2n}$                              | $A_c/A_h\rho_c$                   | 2.52(13)     | 2.52(5)   |
| $R_{c-2n}$                            | $\rho_c + R_{2n}$                 | 3.79(14)     | 3.84(6)   |
| $R_{\text{di-n}}$                     | $(R_h^2 - R_{2n}^2)^{1/2}$        | 2.09(25)     |           |
| $R_{n-n}$                             | $2R_{\text{di-n}}$                | 4.19(49)     | 3.93(25)  |
| $\mathbf{R}_{n1}\cdot\mathbf{R}_{n2}$ | $(A_c^2\rho_c^2 - R_{n-n}^2)/4$   | 1.99(119)    | 2.70(97)  |

- The distance  $R_{n-n}$  between the two halo neutrons is given by

$$R_{n-n} = 2R_{\text{di-n}}, \text{ where } R_h^2 = R_{2n}^2 + R_{\text{di-n}}^2. \quad (29)$$

- The radial correlation of the two halo neutrons is determined as

$$\mathbf{R}_{n1}\cdot\mathbf{R}_{n2} = (A_c^2\rho_c^2 - R_{n-n}^2)/4. \quad (30)$$

The results obtained for the considered geometrical model of  ${}^6\text{He}$  are summarized in Table IV, and one can see a good agreement of our results with those determined in Ref. [3]. Despite the simplicity, the considered geometrical model gives a good illustration of the core movement inside a 2-neutron halo nucleus, which can be estimated by the difference between the core matter radius and that of the free core nucleus. For the  $\alpha$ -core this is just the difference between the proton radius of the free  $\alpha$ -particle and that of the considered halo nucleus because protons are distributed in the  $\alpha$ -core only. In a similar manner, one might suggest the geometry for  ${}^8\text{He}$ , but in this case 4 halo neutrons are distributed uniformly against the  $\alpha$ -core, and the polarizing contributions of the valence neutrons to the motion

of the  $\alpha$ -core should be weaker than that found in the case of  ${}^6\text{He}$ . A direct consequence is a smaller core radius of  ${}^8\text{He}$  compared to that of  ${}^6\text{He}$  as found in the present GSM analysis. It is noted that the  ${}^8\text{He}$  geometry can be considered to have 2 halo neutrons [24]. In this case, the same procedure is applied to determine the nuclear radii as discussed above but now the compact core is  ${}^6\text{He}$ .

## V. SUMMARY

The detailed GSM analysis of the latest experimental data of the elastic  ${}^{6,8}\text{He}+p$  scattering at 717 and 674 MeV/u has been performed. Based on the new data points measured up to the first diffractive minimum, the nuclear radii as well as the radial shape of the matter distribution of these helium halo nuclei have been determined, and the results are in a sound agreement with the recent systematics of these quantities given in Ref. [3].

The sensitivity of the new data points taken at large momentum transfer to the core radius of the  ${}^{6,8}\text{He}$  nuclei as well as to the spin-orbital term in the GSM calculation was demonstrated. The combined data set taken at both low and high momentum transfer were used to fine-tune the parameters of the nuclear densities of  ${}^{6,8}\text{He}$  based on the cluster-orbital shell-model approximation [23].

The core and halo radii obtained from the present GSM analysis were used in a geometrical model suggested for the Borromean nucleus  ${}^6\text{He}$  [3] to determine various size parameters of this nucleus, and the results agree with those obtained in Ref. [3]. The enhancement of the  $\alpha$ -core radius of  ${}^6\text{He}$  compared to that of  ${}^8\text{He}$  found in the present GSM analysis can be qualitatively understood in that simple geometrical picture.

## ACKNOWLEDGMENTS

The present research has been supported, in part, by the National Foundation for Science and Technology Development (NAFOSTED project No.103.04-2014.76) and by the Ministry of Science and Technology of Vietnam (project No.105/2013/HD–NDT). We are grateful to Prof. G.D. Alkhazov and authors of Ref. [10] for providing us with the earlier version of the GSM code, based on which we have developed the present version that includes the

spin-orbital amplitude.

---

- [1] I. Tanihata *et al.*, Phys. Lett. B **206**, 592 (1988).
- [2] I. Tanihata, J. Phys. G **22**, 157 (1996) and references therein.
- [3] I. Tanihata, H. Savajols, and R. Kanungo, Prog. Part. Nucl. Phys. **68**, 215 (2013).
- [4] G.D. Alkhazov *et al.*, Phys. Rev. Lett. **78**, 2313 (1997).
- [5] P. Egelhof, Prog. Part. Nucl. Phys. **46**, 307 (2001).
- [6] A.V. Dobrovolsky *et al.*, Nucl. Phys. A **766**, 1 (2006).
- [7] S. Ilieva *et al.*, Nucl. Phys. A **875**, 8 (2012).
- [8] S.R. Neumaier *et al.*, Nucl. Phys. A **712**, 247 (2002).
- [9] G.D. Alkhazov *et al.*, Phys. Rep. C **42**, 89 (1978).
- [10] G.D. Alkhazov *et al.*, Nucl. Phys. A **712**, 269 (2002).
- [11] J.S. Al-Khalili and J.A. Tostevin, Phys. Rev. C **57**, 1846 (1998).
- [12] O.A. Kiselev *et al.*, Nucl. Instr. and Meth. A **641**, 72 (2011).
- [13] R. Hagedorn, *Relativistic kinematics*, W.A. Benjamin, New York, 1963.
- [14] R.J. Glauber and G. Matthiae, Nucl. Phys. B **21**, 135 (1970).
- [15] O.G. Grebenjuk *et al.*, Nucl. Phys. A **500**, 673 (1989).
- [16] J.P. Auger *et al.*, Nucl. Phys. A **262**, 372 (1976).
- [17] L. Ray, Phys. Rev. C **20**, 1857 (1979).
- [18] Göran Fäldt and Igemar Hulthage, J. Phys. G **4**, 3 (1978).
- [19] L. Ray, G. W. Hoffmann, G. S. Blanpied, W. R. Coker and R. P. Liljestrand, Phys. Rev. C **18**, 1756 (1978).
- [20] D.T. Khoa, E. Khan, G. Coló, and N.V. Giai, Nucl. Phys. A **706**, 61 (2002).
- [21] M.A. Franey and W.G. Love, Phys. Rev. C **31**, 488 (1985).
- [22] P. Mueller *et al.*, Phys. Rev. Lett. **99**, 252501 (2007).
- [23] A.A Korsheninikov *et al.*, Nucl. Phys. A **617**, 45 (1997).
- [24] L. V. Chulkov *et al.*, Nucl. Phys. A **759** 43 (2005).